International Tables for Crystallography (2006). Vol. C, Section 4.2.1, pp. 191–200.

4.2. X-rays

By U. W. Arndt, D. C. Creagh, R. D. Deslattes, J. H. Hubbell, P. Indelicato, E. G. Kessler Jr and E. Lindroth

4.2.1. Generation of X-rays (By U. W. Arndt)

X-rays are produced by the interaction of charged particles with an electromagnetic field. There are four sources of X-rays that are of interest to the crystallographer.

(1) The bombardment of a target by electrons produces a continuous ('white') X-ray spectrum, called *Bremsstrahlung*, which is accompanied by a number of discrete spectral lines characteristic of the target material. The high-vacuum, or Coolidge, X-ray tube is the most important X-ray source for crystallographic studies.

(2) The decay of natural or artificial radio isotopes is often accompanied by the emission of X-rays. Radioactive X-ray sources are often used for the calibration of X-ray detectors. Mössbauer sources have the narrowest known spectral bandwidth and are used in nuclear resonance scattering studies.

(3) Sources of synchrotron radiation produced by relativistic electrons in orbital motion are of growing importance.

(4) X-rays are also produced in plasmas generated by the bombardment of targets by high-energy laser beams, but to date the yield has been principally in the form of soft X-rays.

The classical text on the generation and properties of X-rays is that by Compton & Allison (1935), which still summarizes much of the information required by crystallographers. There is a more recent comprehensive book by Dyson (1973). X-ray physics has received a new impetus on the one hand through the development of X-ray microprobe analysis dealt with in a number of monographs (Reed, 1975; Scott & Love, 1983) and on the other hand through the increasing utilization of synchrotron-radiation sources (see Subsection 4.2.1.5).

4.2.1.1. *The characteristic line spectrum*

Characteristic X-ray emission originates from the radiative decay of electronically highly excited states of matter. We are concerned mostly with excitation by electron bombardment of a target that results in the emission of spectral lines characteristic of the target elements. The electronic states occurring as initial and final states of a process involving the absorption of emission of X-rays are called *X-ray levels*. Levels involving the removal of one electron from the configuration of the neutral ground state are called *normal X-ray levels* or *diagram levels*.

Table 4.2.1.1 shows the relation between diagram levels and electron configurations. The notation used here is the IUPAC notation (Jenkins, Manne, Robin & Senemaud, 1991), which uses arabic instead of the former roman subscripts for the levels. The IUPAC recommendations are to refer to X-ray lines by writing the initial and final levels separated by a hyphen, *e.g.* Cu K-L_3 and to abandon the Siegbahn (1925) notation, *e.g.* Cu $K\alpha_1$, which is based on the relative intensities of the lines. The correspondence between the two notations is shown in Table 4.2.1.2. Because this substitution has not yet become common practice, however, the Siegbahn notation is retained in Section 4.2.2, in which the wavelengths of the characteristic emission lines and absorption edges are discussed.

4.2.1.1.1. *The intensity of characteristic lines*

The efficiency of the production of characteristic radiation has been calculated by a number of authors (see, for example, Dyson, 1973, Chap. 3). For a particular line, it depends on the fluorescence yield, that is the probability that the decay of an excited state leads to the emission of a photon, on the statistical weights of the X-ray levels involved, on the effects of the penetration and slowing down of the bombarding electrons in the target, on the fraction of electrons back-scattered out of the target, and on the contribution caused by fluorescent X-rays produced indirectly by the continuous spectrum. The *emerging* X-ray intensity is further affected by the partial absorption of the generated X-rays in the target.

Dyson (1973) has also reviewed calculations and measurements made of the *relative* intensities of different lines in the K spectrum. The ratio of the $K\alpha_2$ to $K\alpha_3$ intensities is very close to

Table 4.2.1.1. *Correspondence between X-ray diagram levels and electron configurations; from Jenkins, Manne, Robin & Senemaud (1991), courtesy of IUPAC*

Level	Electron configuration	Level	Electron configuration	Level	Electron configuration
K	$1s^{-1}$	N_1	$4s^{-1}$	O_1	$5s^{-1}$
L_1	$2s^{-1}$	N_2	$4p_{1/2}^{-1}$	O_2	$5p_{1/2}^{-1}$
L_2	$2p_{1/2}^{-1}$	N_3	$4p_{3/2}^{-1}$	O_3	$5p_{3/2}^{-1}$
L_3	$2p_{3/2}^{-1}$	N_4	$4d_{3/2}^{-1}$	O_4	$5d_{3/2}^{-1}$
M_1	$3s^{-1}$	N_5	$4d_{5/2}^{-1}$	O_5	$5d_{5/2}^{-1}$
M_2	$3p_{1/2}^{-1}$	N_6	$4f_{5/2}^{-1}$	O_6	$5f_{5/2}^{-1}$
M_3	$3p_{3/2}^{-1}$	N_7	$4f_{7/2}^{-1}$	O_7	$5f_{7/2}^{-1}$
M_4	$3d_{3/2}^{-1}$				
M_5	$3d_{5/2}^{-1}$				

Table 4.2.1.2. *Correspondence between IUPAC and Siegbahn notations for X-ray diagram lines; from Jenkins, Manne, Robin & Senemaud (1991), courtesy of IUPAC*

Siegbahn	IUPAC	Siegbahn	IUPAC	Siegbahn	IUPAC
$K\alpha_1$	K-L_3	$L\alpha_1$	L_3-M_5	$L\gamma_1$	L_2-N_4
$K\alpha_2$	K-L_2	$L\alpha_2$	L_3-M_4	$L\gamma_2$	L_1-N_2
$K\beta_1$	K-M_3	$L\beta_1$	L_2-M_4	$L\gamma_3$	L_1-N_3
$K\beta_2^{\rm I}$	K-N_3	$L\beta_2$	L_3-N_5	$L\gamma_4$	L_1-O_3
$K\beta_2^{\rm II}$	K-N_2	$L\beta_3$	L_1-M_3	$L\gamma_4'$	L_1-O_2
$K\beta_3$	K-M_2	$L\beta_4$	L_1-M_2	$L\gamma_5$	L_2-N_1
$K\beta_4^{\rm I}$	K-N_5	$L\beta_5$	L_3-$O_{4,5}$	$L\gamma_6$	L_2-O_4
$K\beta_4^{\rm II}$	K-N_4	$L\beta_6$	L_3-N_1	$L\gamma_8$	L_2-O_1
$K\beta_{4x}$	K-N_4	$L\beta_7$	L_3-O_1	$L\gamma_8'$	L_2-$N_{6(7)}$
$K\beta_5^{\rm I}$	K-M_5	$L\beta_7'$	L_3-$N_{6,7}$	L_η	L_2-M_1
$K\beta_5^{\rm II}$	K-M_4	$L\beta_9$	L_1-M_5	Ll	L_3-M_1
		$L\beta_{10}$	L_1-M_4	Ls	L_3-M_3
		$L\beta_{15}$	L_3-N_4	Lt	L_3-M_2
		$L\beta_{17}$	L_2-M_3	Lu	L_3-$N_{6,7}$
				Lv	L_2-$N_{6(7)}$

Siegbahn	IUPAC
$M\alpha_1$	M_5-N_7
$M\alpha_2$	M_5-N_6
$M\beta$	M_4-N_6
$M\gamma$	M_3-N_5
$M\zeta$	$M_{4,5}$-$N_{2,3}$

In the case of unresolved lines, such as K-L_2 and K-L_3, the recommended IUPAC notation is K-$L_{2,3}$.

0.5 for Z between 23 and 48. The ratio of $K\beta_3$ to $K\alpha_2$ rises fairly linearly with Z from 0.2 at $Z = 20$ to 0.4 at $Z = 80$ and that of $K\beta_1$ to $K\alpha_2$ is near zero at $Z = 29$ and rises linearly with Z to about 0.1 at $Z = 80$. Relative intensities of lines in the L spectrum are given by Goldberg (1961).

Green & Cosslett (1968) have made extensive measurements of the efficiency of the production of characteristic radiation for a number of targets and for a range of electron accelerating voltages. Their results can be expressed empirically in the form

$$N_K/4\pi = N_0/4\pi(E_0 - E_K - 1)^{1.63}, \qquad (4.2.1.1)$$

where $N_K/4\pi$ is the *generated* number of $K\alpha$ photons per steradian per incident electron, N_0 is a function of the atomic number of the target, E_0 is the electron energy in keV and E_K is the excitation potential in keV. It should be noted that $N_K/4\pi$ decreases with increasing Z.

For a copper target, this expression becomes

$$N_K/4\pi = 1.8 \times 10^{-6}\,(E_0 - 8.9)^{1.63} \qquad (4.2.1.2)$$

or

$$N'_K/4\pi = 1.1 \times 10^{10}\,(E_0 - 8.9)^{1.63}, \qquad (4.2.1.3)$$

where $N'_K/4\pi$ is the number of $K\alpha$ photons per steradian per second per milliampere of tube current.

These expressions are probably accurate to within a factor of 2 up to values of E_0/E_K of about 10. Guo & Wu (1985) found a linear relationship for the *emerging* number of photons with electron energy in the range $2 < E_0/E_K < 5$.

To obtain the number of photons that *emerge* from the target, the above expressions have to be corrected for absorption of the generated radiation in the target. The number of photons emerging at an angle φ to the surface, for normal electron incidence, is usually written

$$N_\varphi/4\pi = f(\chi)N/4\pi, \qquad (4.2.1.4)$$

where $\chi = (\mu/\rho)\,\mathrm{cosec}\,\varphi$ (Castaing & Descamps, 1955). Green (1963) gives experimental values of the correction factor $f(\chi)$ for a series of targets over a range of electron energies. His curves for a copper target are given in Fig. 4.2.1.1. It will be noticed that the correction factor increases with increasing electron energy since the effective depth of X-ray generation increases with voltage. As a result, curves of N_φ as a function of E_0 have a broad maximum that is displaced towards lower voltages as φ decreases, as shown in the experimental curves for copper K radiation due to Metchnik & Tomlin (1963) (Fig. 4.2.1.2). For very small take-off angles, therefore, X-ray tubes should be operated at lower than customary voltages. Note that the values in Fig. 4.2.1.2 agree to within $\sim 40\%$ with those of Green & Cosslett. $f(\chi)$ at constant E_0/E_K increases with increasing Z, thus partly compensating for the decrease in N_K, especially at small values of φ. A recent re-examination of the characteristic X-ray flux from Cr, Cu, Mo, Ag and W targets has been carried out by Honkimaki, Sleight & Suortti (1990).

4.2.1.2. *The continuous spectrum*

The shape of the continuous spectrum from a thick target is very simple: I_ν, the energy per unit frequency band in the spectrum, is given by the expression derived by Kramers (1923):

$$I_\nu = AZ(\nu_0 - \nu) + BZ^2, \qquad (4.2.1.5)$$

where Z is the atomic number of the target and A and B are constants independent of the applied voltage E_0. B/A is of the order of 0.0025 so that the term in Z^2 can usually be neglected (Fig. 4.2.1.3). ν_0 is the maximum frequency in the spectrum, *i.e.* the Duane–Hunt limit at which the entire energy of the bombarding electrons is converted into the quantum energy of the emitted photon, where

$$H\nu_0 = hc/\lambda_0 = E_0. \qquad (4.2.1.6)$$

Using the latest adjusted values of the fundamental constants (Cohen & Taylor, 1987):

$$hc = 1.23984244 \pm 0.00000037 \times 10^{-6}\ \text{eV m}$$
$$= 12.3984244 \pm 0.0000037\ \text{keV Å}.$$

Equation (4.2.1.5) can be rewritten in a number of forms. If $\mathrm{d}N_E$ is the number of photons of energy E per incident electron,

$$\mathrm{d}N_E = bZ(E_0/E - 1)\ \mathrm{d}E, \qquad (4.2.1.7)$$

where $b \sim 2 \times 10^{-9}$ photons eV^{-1} $\mathrm{electron}^{-1}$, and is known as Kramer's constant.

From (4.2.1.7), it follows that the total energy in the continuous spectrum per electron is

$$\int_0^{E_0} E\ \mathrm{d}N_E = bZE_0^2/2. \qquad (4.2.1.8)$$

Since the energy of the bombarding electron is E_0, the efficiency of production of the continuous radiation is

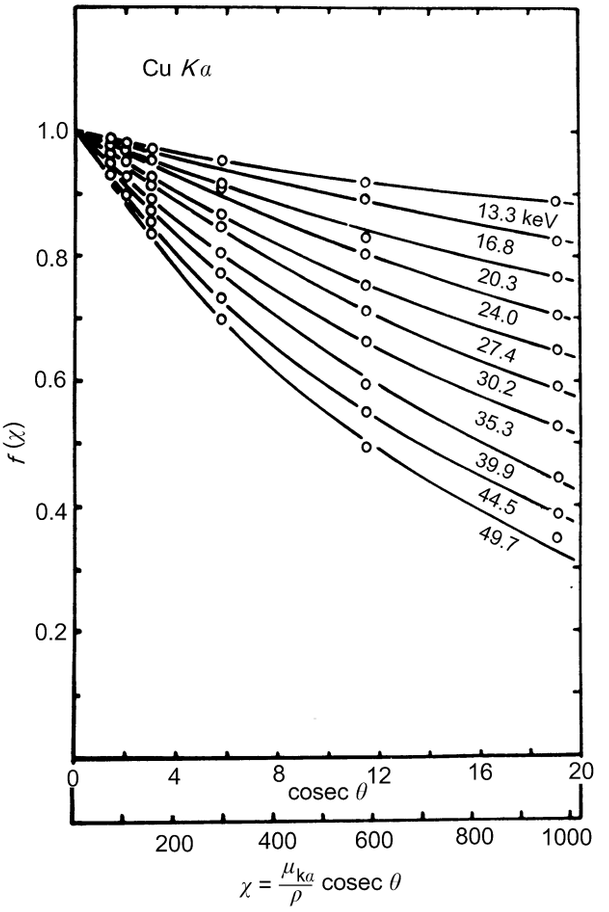

Fig. 4.2.1.1. $f(\chi)$ curves for Cu K-L_3 at a series of different accelerating voltages (in kV). From Green (1963).

$$\eta_c = bZE_0/2. \quad (4.2.1.9)$$

Crystallographers are more accustomed to thinking of the spectrum in terms of wavelength. Equation (4.2.1.7) can be transformed into

$$dN_\lambda = hcbZ(1/\lambda^2 - 1/\lambda\lambda_0)\, d\lambda, \quad (4.2.1.10)$$

which has a maximum at $\lambda = 2\lambda_0$. In practice, the *emerging* spectrum is modified by target absorption, which is greatest for the longer wavelengths and moves the maximum more nearly to $1.5\lambda_0$.

It is of interest to compare the X-ray flux in a narrow wavelength band selected by an appropriate monochromator with the flux in a characteristic spectral line, in order to examine the practicability of XAFS (X-ray absorption fine-structure spectroscopy) or optimized anomalous-dispersion diffractometry experiments. For these purposes, the maximum permissible wavelength band is about 10^{-3} Å. From equation (4.2.1.10), we see that, for a tungsten-target X-ray tube operated at 80 kV, dN_λ is about 1.1×10^{-5} photons with the $K\alpha$ energy electron^{-1} steradian^{-1} $(10^{-3}\,\delta\lambda/\lambda)^{-1}$ for an X-ray wavelength in the neighbourhood of 1.5 Å. By comparison, from equation (4.2.1.2), a copper-target tube operated at 40 kV produces about 5×10^{-4} $K\alpha$ photons electron^{-1} steradian^{-1}. In spite of this shortcoming by a factor of about 45, laboratory XAFS experiments are sufficiently common to have merited at least one specialized conference (Stern, 1980; see also Tohji, Udagawa, Kawasaki & Masuda, 1983; Sakurai, 1993; Sakurai & Sakurai, 1994).

The use of continuous radiation for diffraction experiments is complicated by the fact that the radiation is polarized. The degree of polarization may be defined as

$$p = (I_\parallel - I_\perp)/(I_\parallel + I_\perp), \quad (4.2.1.11)$$

where $I_\parallel$ and $I_\perp$ are the intensities of radiation with the electric vector parallel and perpendicular to the plane containing the incident electrons and the direction of the emitted photons. For an angle of $\pi/2$ between the electrons and the emitted beam, p varies smoothly through the spectrum; it is negative for the softest radiation, approximately zero at $\nu/\nu_0 \sim 0.1$ and reaches values between +0.7 and +0.9 near the Duane–Hunt limit (Kirkpatrick & Wiedmann, 1945). Since practical use of white radiation is likely to be in the vicinity of $\nu/\nu_0 \sim 0.1$, the effect is not a large one.

It should also be noted that the spatial distribution of the white spectrum, even after correction for absorption in the target, is not isotropic. The intensity has a maximum at about 50° to the electron beam and non-zero minima at 0 and 180° to that beam (Stephenson, 1957).

4.2.1.3. *X-ray tubes*

The commonest source of X-rays is the high-vacuum, or Coolidge, X-ray tube, which may be either demountable and pumped continuously when in operation or permanently sealed after evacuation. The vacuum tube contains an electron gun that incorporates a thermionic cathode, which produces a well defined electron beam that is accelerated towards the anode or target, formerly often called the anticathode. In most X-ray tubes intended for crystallographic purposes, the anode is massive, *i.e.* its thickness is large compared with the range of the electrons; it is usually water-cooled and its surface is normal to the incident electron beam. Usually, it is desirable for the X-ray source to be small (between 25 μm and 1 mm square) and for the X-ray intensity from the tube to be the maximum possible for the amount of power that can be dissipated in the target. These objectives are best achieved by

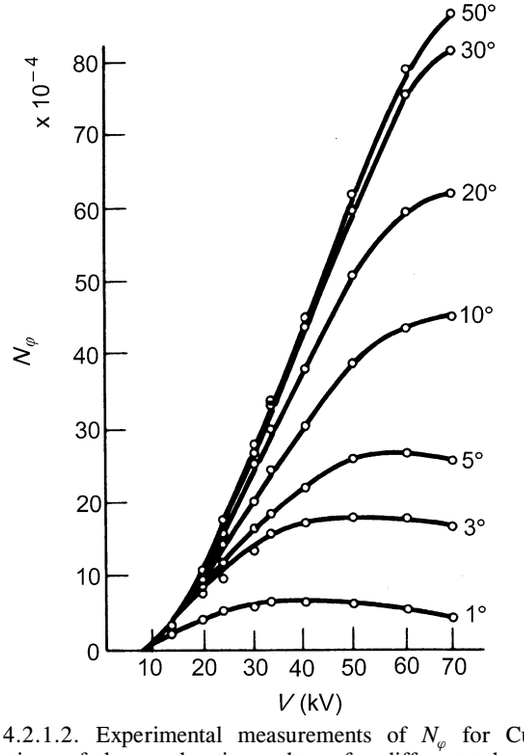

Fig. 4.2.1.2. Experimental measurements of N_φ for Cu K-L_3 as functions of the accelerating voltage for different take-off angles. From Metchnik & Tomlin (1963).

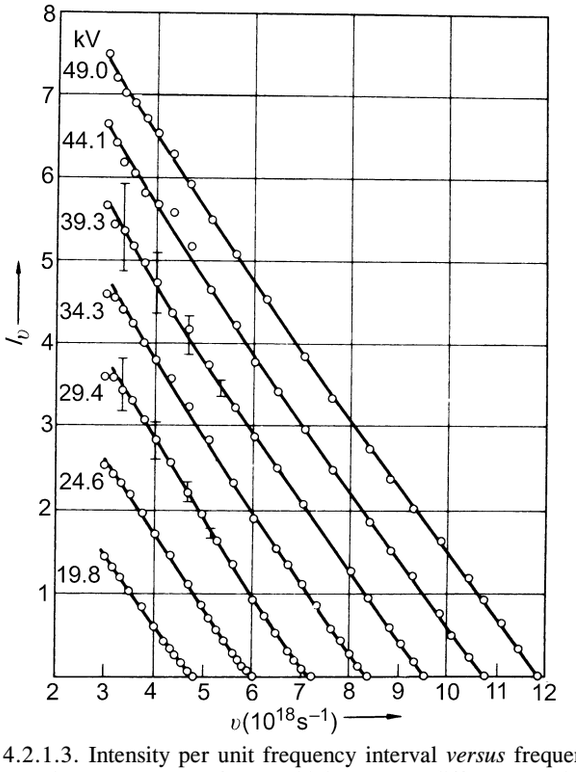

Fig. 4.2.1.3. Intensity per unit frequency interval *versus* frequency in the continuous spectrum from a thick target at different accelerating voltages. From Kuhlenkampff & Schmidt (1943).

Table 4.2.1.3. *Copper-target X-ray tubes and their loading*

X-ray tube	Anode diameter (mm)	Speed		$f_1 \times f_2$ (mm) (mm)	μ	Loading (kW)		Recommended specific loading (kW mm^{-2})
		r min^{-1}	mm s^{-1}			calc.	recommended	
Standard insert	–	–	–	8×0.15	0.295	1.0	0.8	0.67
	–	–	–	8×0.4	0.359	1.2	1.5	0.47
	–	–	–	10×1.0	0.425	1.8	2.0	0.20
	–	–	–	12×2.0	0.493	2.5	2.7	0.11
AEI-GX21	89	6000	28000	1×0.1	0.425	1.4	1.2	12.0
				2×0.2	0.425	3.95	3.2	8.0
				3×0.3	0.425	7.3	5.2	5.8
				5×0.5	0.425	15.6	15.0	6.0
AEI-GX13	457	4500	108000	1×0.1	0.425	2.7	2.7	27.0
Rigaku-RU200	99	6000	31000	1×0.1	0.425	1.5	1.2	12.0
				2×0.2	0.425	4.2	3.0	7.5
				3×0.3	0.425	7.6	5.4	6.0
Rigaku-RU500	400	1250	26200	10×0.5	0.359	26.8	30	6.0
Rigaku-RU1000	400	2500	52450	10×1	0.425	60	60	6.0
Rigaku-RU1500	250	10000	131000	10×1	0.425	96	90	9.0
KFA-Jülich	250	12000	157000	14×1.4	0.425	173	120	6.1

designing the electron gun to produce a line focus, that is the electron focus on the target face is approximately rectangular with the small dimension equal to the desired effective source size and the large dimension about 10 to 20 times larger. The focus is viewed at an angle between about 2 and 5° to the anode surface to produce an approximately square foreshortened effective source; and the X-ray windows are so positioned as to make these take-off angles possible. For some purposes, very fine line sources are required and windows may be provided to allow the focus to be viewed so as to foreshorten the line width. Higher power dissipation is possible in X-ray tubes in which the anode rotates: the line focus is now usually on the cylindrical surface of the anode with its long dimension parallel to the axis of rotation.

For focal-spot sizes down to about 100 μm, an electrostatic gun is adequate; this consists of a fine helical filament and a Wehnelt cathode, which produces a demagnified electron image of the filament on the anode. For most purposes, the Wehnelt cathode can be at the same potential as the filament but cleaner foci and adjustment of the focal spot size are possible when this electrode is negatively biased with respect to the filament. The filament is nearly always directly heated and made of tungsten. Lower filament temperatures, and smaller heating currents, could be achieved with activated heaters but the vacuum in high-power devices like X-ray tubes is rarely hard enough to permit their use since they are easily poisoned. However, Yao (1992) has reported successful operation of a hot-pressed polycrystalline lanthanum hexaboride cathode in an otherwise unmodified RU-1000 rotating-target X-ray generator.

Very fine focus tubes, with foci in the range between 25 and 1 μm, require magnetic lenses. At one time, the all-electrostatic X-ray tube of Ehrenberg & Spear (1951), which achieved foci between 20 and 80 μm, was very popular.

Sealed-off X-ray tubes for crystallographic use are nowadays made in the form of inserts containing a target of one of a range of standard metals to produce the desired characteristic radiation. A series of nominal focal-spot sizes, shown in Table 4.2.1.3, is commonly available. The insert is mounted inside a standard shield that is radiation- and shock-proof and that is fitted with X-ray shutters and filters and often also with a standardized track for mounting X-ray cameras. The water-cooled anode is normally at ground potential and the negative high voltage for the cathode, together with the filament supply, is brought in through a shielded shock-proof cable. The high voltage is nowadays generally of the constant-voltage type, that is, it is full-wave rectified and smoothed by means of solid-state rectifiers and capacitors housed in the high-voltage transformer tank, which also contains the filament transformer. The high tension and the tube current are frequently stabilized. Only the simplest X-ray generators now employ an alternating high tension that is rectified by the self-rectifying property of the X-ray tube itself.

A demountable continuously pumped form of construction is nowadays adopted mainly for rotating-anode and other specialized X-ray tubes. The pumping system must be capable of maintaining a vacuum of better than 10^{-5} Torr: filament life is critically dependent upon the quality of the vacuum.

Rotating-anode tubes have been reviewed by Yoshimatsu & Kozaki (1977). The first successful tube of this type that incorporated a vacuum shaft seal was described by Clay (1934). Modern tubes mostly contain vacuum-oil-lubricated shaft seals of the type due to Wilson (1941) and are based on, or are similar to, the rotating-anode tubes described by Taylor (1949, 1956). In some tubes, successful use has been made of ferro-fluidic vacuum seals (see Bailey, 1978). The main problems in the operation of rotating-anode tubes is the lifetime of the seals and of bearings that operate *in vacuo*. In successful tubes, *e.g.* those

manufactured by Enraf, Rigaku-Denki, and Siemens, these lifetimes are about the same as the lifetime of the filament under good vacuum conditions, that is, of the order of 1000 h.

Phillips (1985) has written a review article on stationary and rotating-anode X-ray tubes that contains many important practical details.

4.2.1.3.1. *Power dissipation in the anode*

The allowable power loading of X-ray tube targets is determined by the temperature of the target surface, which must remain below the melting point. Müller (1927, 1929, 1931) first calculated the maximum loading both for stationary and for rotating anodes. His calculations were refined by Oosterkamp (1948) who considered, in particular, targets of finite thickness, and who also treated pulsed operation of the tube. For normal conditions, Oosterkamp's conclusions and those of Ishimura, Shiraiwa & Sawada (1957) do not greatly differ from those of Müller, which are in adequate agreement with experimental observations.

For an elliptical focal spot with axes f_1 and f_2, Müller's formula for the maximum power dissipation on a stationary anode, assumed to be a water-cooled block of dimensions large compared with the focal-spot dimensions, can be written

$$W_{\rm stat} = 2.063(T_M - T_0)Kf_1\mu(f_1,f_2), \qquad (4.2.1.12)$$

where K is the specific thermal conductivity of the target material in $\mathrm{W\,mm^{-1}}$, T_M is the maximum temperature at the centre of the focal spot on the target, that is, a temperature well below the melting point of the target material, and T_0 is the temperature of the cold surface of the target, that is, of the cooling water. The function μ is shown in Fig. 4.2.1.4. For copper, K is $400\,\mathrm{W\,m^{-1}}$ and, with $T_M - T_0 = 500\,\mathrm{K}$,

$$W_{\rm stat} = 425\mu f_1. \qquad (4.2.1.13)$$

For $f_2/f_1 = 0.1$, and $\mu = 0.425$, this equation becomes

$$W_{\rm stat} = 180 f_1. \qquad (4.2.1.14)$$

In these last two equations, f_1 is in mm.

For a rotating target, Müller found that the permissible power dissipation was given by

$$W_{\rm rot} = 1.428\,K(T_M - T_0)f_1(f_2\rho Cv/2K)^{1/2}, \qquad (4.2.1.15)$$

where f_2 is the short dimension of the focus, assumed to be in the direction of motion of the target, v is the linear velocity, ρ is the density of the target material, and C is its specific heat.

For a copper target with f_1 and f_2 in mm and v in $\mathrm{mm\,s^{-1}}$,

$$W_{\rm rot} = 26.4 f_1(f_2 v)^{1/2}. \qquad (4.2.1.16)$$

Equation (4.2.1.16) shows that for very narrow focal spots rotating-anode tubes give useful improvements in permissible loading only if the surface speed is very high (see Table 4.2.1.3). The reason is that with large foci on stationary anodes the isothermal surfaces in the target are planar; with fine foci, these surfaces become cylindrical and this already makes for very efficient cooling without the need for rotation. Rotating anodes are thus most useful for medium-size foci (200 to 500 μm) since for the larger focal spots it becomes very expensive to construct power supplies capable of supplying the permissible amount of power.

Table 4.2.1.3 shows the recommended loading for a number of commercially available X-ray tubes with copper targets, which will be seen to be in qualitative agreement with the calculations. Some of the discrepancy is due to the fact that the value of $K(T_M - T_0)$ for the copper–chromium alloy targets used in actual X-ray tubes is appreciably lower than the value for pure copper used here. To a good approximation, the permissible loading for other targets can be derived by multiplying those in Table 4.2.1.3 by the factors shown in Table 4.2.1.4. It is worth noting that the recommended loading of commercial stationary-target X-ray tubes has increased steadily in recent years. This is largely due to improvements in the water cooling of the back surface of the target by increasing the turbulence of the water and the effective surface area of the cooled surface.

In considering Table 4.2.1.3, it should be noted that the linear velocities of the highest-power X-ray-tube anode have already reached a speed that Yoshimatsu & Kozaki (1977) consider the practical limit, which is set by the mechanical properties of engineering materials. It should also be noted that much higher specific loads can be achieved for true micro-focus tubes, *e.g.* $50\,\mathrm{kW\,mm^{-2}}$ for a 25 μm Ehrenberg & Spear tube and $1000\,\mathrm{kW\,mm^{-2}}$ for a tube with a 1 μm focus (Goldsztaub, 1947; Cosslett & Nixon, 1951, 1960).

Some tubes with focus spots of less than 10 μm utilize foil or needle targets. These targets and the heat dissipated in them have been discussed by Cosslett & Nixon (1960). The dissipation is less than that in a massive target by a factor of about 3 for a foil and 10 for a needle, but, in view of the low absolute power, target movement and even water-cooling can be dispensed with.

4.2.1.4. *Radioactive X-ray sources*

Radioactive sources of X-rays are mainly of interest to crystallographers for the calibration of X-ray detectors where they have the great advantage of being completely stable with time, or at least of having an accurately known decay rate. For some purposes, spectral purity of the radiation is important; radionuclides that decay wholly by electron capture are particularly useful as they produce little or no β or other radiation. In this type of decay, the atomic number of the daughter nucleus is one less than that of the decaying isotope, and the emitted X-rays are characteristic of the daughter nucleus. In some cases, the probability of electron capture taking place

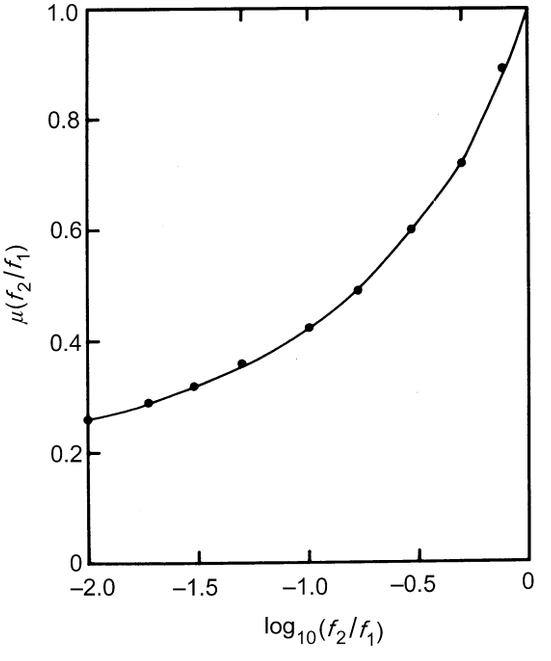

Fig. 4.2.1.4. The function μ in Müller's equation (equation 4.2.1.12) as a function of the ratio of width to length of the focal spot.

Table 4.2.1.4. *Relative permissible loading for different target materials*

Cu	Cr	Fe	Co	Mo	Ag	W
1.0	0.9	0.6	0.9	1.2	1.0	1.2

from some shell other than the K shell is very small and most of the photons emitted are K photons. The number of photons emitted into a solid angle of 4π, uncorrected for absorption, is given by the strength of the source in Curies ($1\,\text{Curie} = 3.7 \times 10^{10}\,\text{disintegrations}\,\text{s}^{-1}$), since each disintegration produces one photon. A list of these nuclei (after Dyson, 1973) is given in Table 4.2.1.5.

Useful radioactive sources are also made by mixing a pure β-emitter with a target material. These sources produce a continuous spectrum in addition to the characteristic line spectrum. The nuclide most commonly used for this purpose is tritium which emits β particles with an energy up to 18 keV and which has a half-life of 12.4 a.

Radioactive X-ray sources have been reviewed by Dyson (1973).

4.2.1.5. *Synchrotron-radiation sources*

The growing importance of synchrotron radiation is attested by a large number of monographs (Kunz, 1979; Winick, 1980; Stuhrmann, 1982; Koch, 1983) and review articles (Godwin, 1968; Kulipanov & Strinskii, 1977; Lea, 1978; Winick & Bienenstock, 1978; Helliwell, 1984; Buras, 1985). Project studies for storage rings such as the European Synchrotron Radiation Facility, the ESRF (Farge & Duke, 1979; Thompson & Poole, 1979; Buras & Marr, 1979; Buras & Tazzari, 1984) are still worth consulting for the reasoning that lay behind the design; the ESRF has, in fact, achieved or even exceeded the design parameters (Laclare, 1994).

A charged particle with energy E and mass m moving in a circular orbit of radius R at a constant speed v radiates a power P into a solid angle of 4π, where

$$P = 2e^2c(v/c)^4(E/mc^2)^4/3R^2. \qquad (4.2.1.17)$$

The orbit of the particle can be maintained only if the energy lost in the form of electromagnetic radiation is constantly replenished. In an electron synchrotron or in a storage ring, the circulating particles are electrons or positrons maintained in a closed orbit by a magnetic field; their energy is supplied or restored by means of an oscillating radio-frequency (RF) electric field at one or more places in the orbit. In a synchrotron, designed for nuclear-physics experiments, the circulating particles are injected from a linear accelerator, accelerated up to full energy by the RF field and then deflected into a target with a cycle frequency of about 50 Hz. The synchrotron radiation is thus produced in the form of pulses of this frequency. A storage ring, on the other hand, is filled with electrons or positrons and after acceleration the particle energy is maintained by the RF field; the current ideally circulates for many hours and decays only as a result of collisions with remaining gas molecules. At present, only storage rings are used as sources of synchrotron radiation and many of these are dedicated entirely to the production of radiation: they are not used at all, or are used only for limited periods, for nuclear-physics collision experiments.

In equation (4.2.1.17), we may substitute for the various constants and obtain for the radiated power

Table 4.2.1.5. *Radionuclides decaying wholly by electron capture, and yielding little or no γ-radiation*

Nuclide	Half-life	X-rays		Remarks
		Element	$K\alpha_1$ (keV)	
^{37}Ar	35 d	Cl	2.622	–
^{51}Cr	27.8 d	V	4.952	γ at 320 keV
^{55}Fe	2.6 a	Mn	5.898	–
^{71}Ge	11.4 d	Ga	9.251	–
^{103}Pd	17 d	Rh	20.214	Several γ's; all weak
^{109}Cd	453 d	Ag	22.16	γ at 88 keV
^{125}I	60 d	Te	27.47	γ at 35.4 keV
^{131}Cs	10 d	Xe	29.80	–
^{145}Pm	17.7a	Nd	37.36	γ's at 67 and 72 keV
^{145}Sm	340 d	Pm	38.65	γ's at 61 keV; weak γ at 485 keV
^{179}Ta	600 d	Hf	55.76	–
^{181}W	140 d	Ta	57.52	γ at 6.5 keV; weak γ's at 136, 153 keV
^{205}Pb	5×10^7a	Tl	L only (L_{α_1} = 10.27 keV)	–

$$P = 0.0885\,E^4I/R, \qquad (4.2.1.18)$$

where E is in GeV (10^9 eV), I is the circulating electron or positron current in milliamperes, and R is in metres. Thus, for example, at the Daresbury storage ring in England, $R = 5.5$ m and, for operation at 2 GeV and 200 mA, $P = 51.5$ kW. Storage rings with a total power of the order of 1 MW are planned.

For relativistic electrons, the electromagnetic radiation is compressed into a fan-shaped beam tangential to the orbit with a vertical opening angle $\psi \simeq mc^2/E$, *i.e.* ~ 0.25 mrad for $E = 2$ GeV (Fig. 4.2.1.5). This fan rotates with circulating electrons: if the ring is filled with n bunches of electrons, a stationary observer will see n flashes of radiation every $2\pi R/c$ s, the duration of each flash being less than 1 ns.

The spectral distribution of synchrotron radiation extends from the infrared to the X-ray region; Schwinger (1949) gives the instantaneous power radiated by a monoenergetic electron in a circular motion per unit wavelength interval as a function of wavelength (Winick, 1980). An important parameter specifying the distribution is the critical wavelength λ_c: half the total power radiated, but only $\sim 9\%$ of the total number of photons, is at $\lambda < \lambda_c$ (Fig. 4.2.1.6). λ_c is given by

$$\lambda_c = 4\pi R/3(E/mc^2)^3, \qquad (4.2.1.19)$$

from which it follows that λ_c in Å can be expressed as

$$\lambda_c = 18.64/(BE^2), \qquad (4.2.1.20)$$

where B ($= 3.34\,E/R$) is the magnetic bending field in T, E is in GeV, and R is in metres.

Synchrotron radiation is highly polarized. In an ideal ring where all electrons are parallel to one another in a central orbit, the radiation in the orbital plane is linearly polarized with the electric vector lying in this plane. Outside the plane, the radiation is elliptically polarized.

In practice, the electron path in a storage ring is not a circle. The 'ring' consists of an alternation of straight sections and bending magnets and beam lines are installed at these magnets.

So-called *insertion devices* with a zero magnetic field integral, *i.e. wigglers* and *undulators*, may be inserted in the straight sections (Fig. 4.2.1.7). A wiggler consists of one or more dipole magnets with alternating magnetic field directions aligned transverse to the orbit. The critical wavelength can thus be shifted towards shorter values because the bending radius can be made small over a short section, especially when superconducting magnets are used. Such a device is called a *wavelength shifter*. If it has N dipoles, the radiation from the different poles is added to give an N-fold increase in intensity. Wigglers can be horizontal or vertical.

In a wiggler, the maximum divergence 2α of the electron beam is much larger than ψ, the vertical aperture of the radiation cone in the spectral region of interest (Fig. 4.2.1.5). If $2\alpha \ll \psi$ and if, in addition, the magnet poles of a multipole device have a short period λ_0, the device becomes an undulator: interference will take place between the radiation emitted at two points λ_0 apart on the electron trajectory (Fig. 4.2.1.8). The spectrum at an angle φ to the axis observed through a pin-hole will consist of a single spectral line and its harmonics of wavelengths

$$\lambda_i = i^{-1}\lambda_0[(E/mc^2)^{-2} + \alpha^2/2 + \theta^2]/2 \qquad (4.2.1.21)$$

(Hofmann, 1978). Typically, the bandwidth of the lines, $\delta\lambda/\lambda$, will be ~ 0.01 to 0.1 and the photon flux per unit band width from the undulator will be many orders of magnitude greater than that from a bending magnet. Existing undulators have been designed for photon energies below 2 keV; higher energies, because of the relatively weak magnetic fields necessitated by the need to keep λ_0 small [equation (4.2.1.21)], require a high electron energy: undulators with a fundamental wavelength in the neighbourhood of 0.86 Å are planned for the European storage ring (Buras & Tazzari, 1984).

The wavelength spectra for a bending magnet, a wiggler and an undulator for the ESRF, are shown in Fig. 4.2.1.9. A comparison of the spectra from an existing storage ring with the spectrum of a rotating-anode tube is shown in Fig. 4.2.1.10.

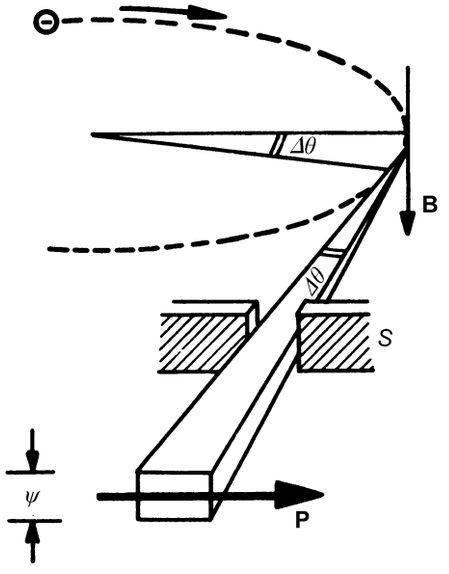

Fig. 4.2.1.5. Synchrotron radiation emitted by a relativistic electron travelling in a curved trajectory. B is the magnetic field perpendicular to the plane of the electron orbit; ψ is the natural opening angle in the vertical plane; P is the direction of polarization. The slit S defines the length of the arc of angle $\Delta\theta$ from which the radiation is taken. From Buras & Tazzari (1984); courtesy of ESRP.

The important properties of synchrotron-radiation sources are:
(1) high intensity;
(2) very broad continuous spectral range;
(3) narrow angular collimation;
(4) small source size;
(5) high degree of polarization;
(6) regularly pulsed time structure;
(7) computability of properties.

Table 4.2.1.6 (after Buras & Tazzari, 1984) compares the most important parameters of the European Synchrotron Radiation Facility (ESRF) with a number of other storage rings. In this table, BM and W signify bending-magnet and wiggler beam lines, respectively, σ_x and σ'_z is the source divergence; the flux is integrated in the vertical plane. The ESRF is seen to have a higher flux than other sources; even more impressive by virtue of the small dimensions of the source size and divergence are its improvements in spectral brightness (defined as the number of photons s^{-1} per unit solid angle per 0.1% bandwidth) and in spectral brilliance (defined as the number of photons s^{-1} per unit solid angle per unit area of the source per 0.1% bandwidth). In comparing different synchrotron-radiation sources with one another and with conventional sources (Fig. 4.2.1.10), the relative quantity for comparison may be flux, brightness or brilliance, depending on the type of diffraction experiment and the type of collimation adopted. Table 4.2.1.7 (due to Farge & Duke, 1979) attempts to compare intensity factors for a number of typical experiments. In general, a high brightness is important in experiments that do not embody focusing elements, such as mirrors or

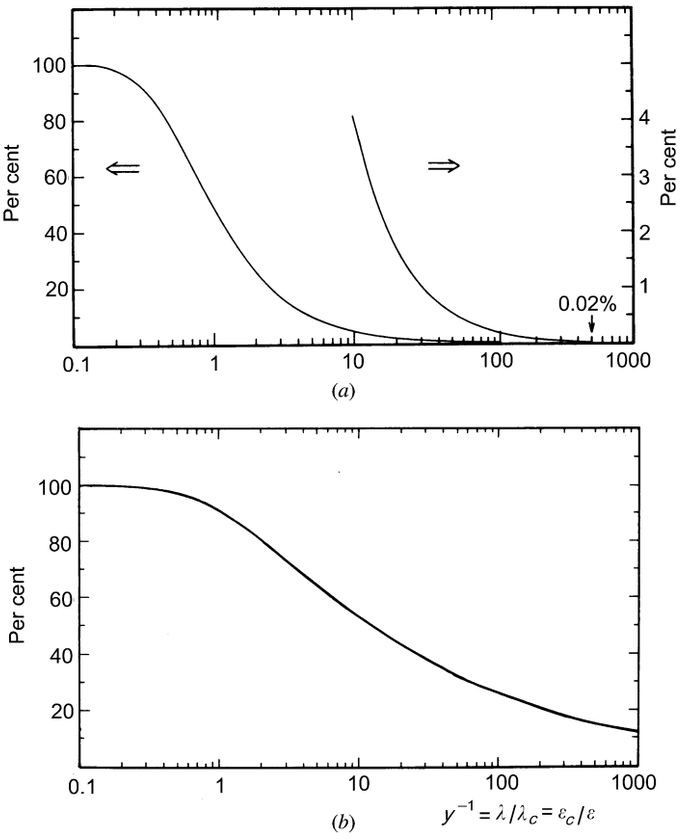

Fig. 4.2.1.6. Synchrotron-radiation spectrum: percentage per unit wavelength interval (*a*) of power of total power and (*b*) of number of photons of total number of photons at wavelengths greater than λ *versus* λ/λ_c. Note that half the power but only 9% of the photons are radiated at wavelengths less than λ_c; courtesy of H. Winick.

curved crystals, and a high brilliance in those experiments that do.

Many surveys of existing and planned synchrotron-radiation sources have been published since the compilation of Table 4.2.1.6. Figure 4.2.1.11, taken from a recent review (Suller, 1992), is a graphical illustration of the growth and the distribution of these sources. An earlier census is due to Huke & Kobayakawa (1989). Many detailed descriptions of beam lines for particular purposes, such as protein crystallography (*e.g* Fourme, 1992) or at individual storage rings (*e.g*. Kusev, Raiko & Skuratowski, 1992) have appeared: these are too numerous to list here and can be located by reference to *Synchrotron Radiation News*.

4.2.1.6. *Plasma X-ray sources*

Plasma sources of hard X-rays are being investigated in many laboratories. Most of the material in this section is derived from publications from the Laboratory for Laser Energetics, University of Rochester, USA. Plasma sources of very soft X-rays have been reviewed by Byer, Kuhn, Reed & Trail (1983).

The peak wavelength of emission from a black-body radiator falls into the ultraviolet at about 10^5 K and into the X-ray region between 10^6 and 10^7 K. At these temperatures, matter is in the form of a plasma that consists of highly ionized atoms and of electrons with energies of several keV. The only successful methods of heating plasmas to temperatures in excess of 10^6 K is by means of high-energy laser beams with intensities of 10^{12} W mm^{-2} or more. The duration of the laser pulse must be less than 1 ns so that the plasma cannot flow away from the pulse. When the plasmas are created from elements with $15 < Z < 25$, they consist mainly of ions stripped to the *K* shell, that is of hydrogen- and helium-like ions. The X-ray spectrum (Fig. 4.2.1.12) then contains a main group of lines with a bandwidth for the group of about 1%; the band is situated slightly below the *K*-absorption edge of the target material. The intensity of the band drops with increasing atomic number. For diffraction studies, Forsyth & Frankel (1980, 1984) and Frankel & Forsyth (1979, 1985) used a multi-stage Nd^{3+}:glass laser (Seka, Soures, Lewis, Bunkenburg, Brown, Jacobs, Mourou & Zimmermann, 1980), which was able to deliver up to 220 J per pulse of width 700 ps. They obtained 6×10^{14} photons pulse^{-1} for a Cl^{15+} plasma with a mean wavelength of about 4.45 Å and about 3×10^{13} photons pulse^{-1} for a Fe^{24+} plasma at about 1.87 Å (Yaakobi, Bourke, Conturie, Delettrez, Forsyth, Frankel, Goldman, McCrory, Seka, Soures, Burek & Deslattes, 1981). More recently, the laser was fitted

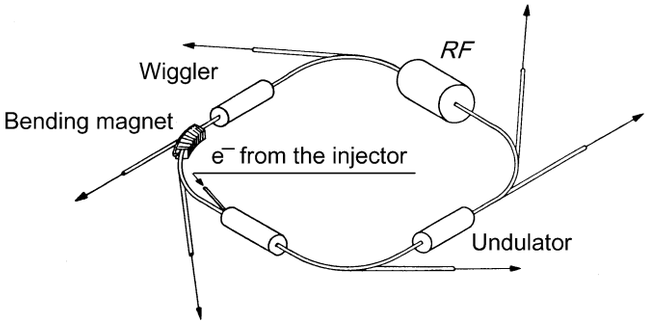

Fig. 4.2.1.7. Main components of a dedicated electron storage-ring synchrotron-radiation source. For clarity, only one bending magnet is shown. From Buras & Tazzari (1984); courtesy of ESRP.

Fig. 4.2.1.8. Electron trajectory within a multipole wiggler or undulator. λ_0 is the spatial period, α the maximum deflection angle, and θ the observation angle. From Buras & Tazzari (1984); courtesy of ESRP.

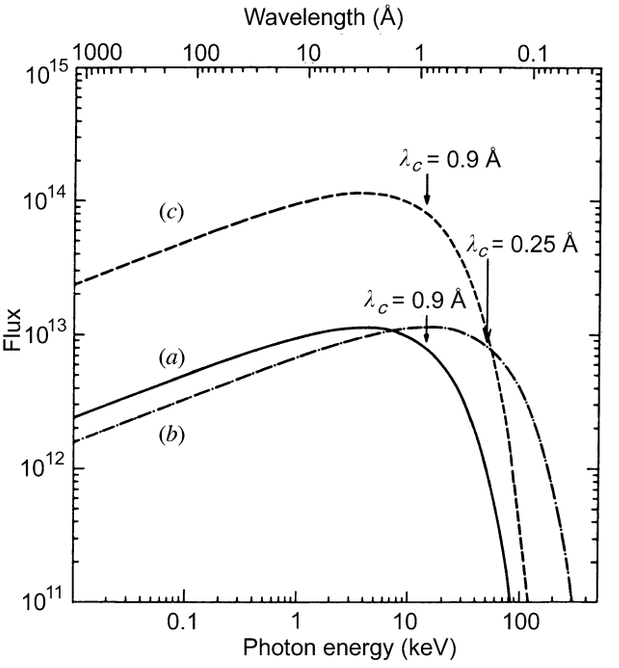

Fig. 4.2.1.9. Spectral distribution and critical wavelengths for (*a*) a dipole magnet, (*b*) a wavelength shifter, and (*c*) a multipole wiggler for the proposed ESRF. From Buras & Tazzari (1984); courtesy of ESRP.

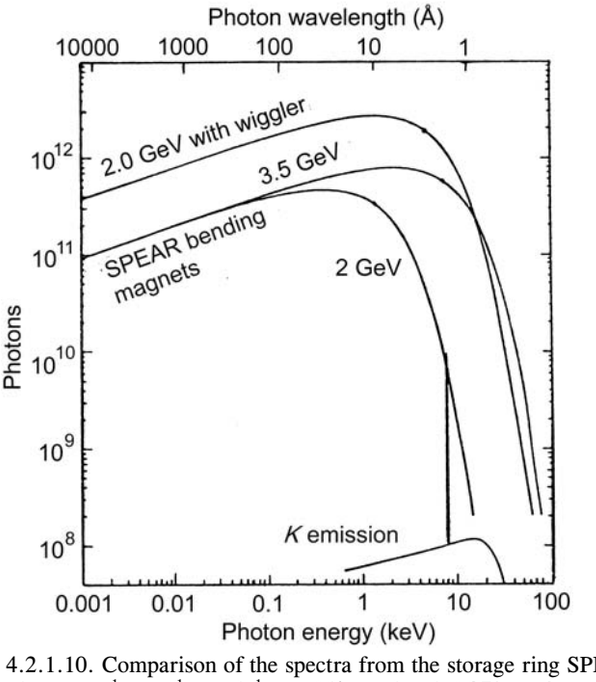

Fig. 4.2.1.10. Comparison of the spectra from the storage ring SPEAR in photons s^{-1} mA^{-1} mrad^{-1} per 1% passband (1978 performance) and a rotating-anode X-ray generator. From Nagel (1980); courtesy of K. O. Hodgson.

Table 4.2.1.6. *Comparison of storage-ring synchrotron-radiation sources; the parameters were correct in 1985 and, for some sources, may be substantially different from those at earlier or later periods; after Buras & Tazzari (1984), courtesy of ESRP*

Storage ring	Source type	No. of poles	I (mA)	E (GeV)	R (m)	σ_x (mm)*	σ_z (mm)*	σ'_z (mrad)*	λ_c (Å)	$E_{c(\mathrm{keV})}$	Flux $\left[\frac{\text{photons s}^{-1}}{\text{mrad} \times 0.1\%\ \text{BW}}\right]$ at λ^c	Flux at 1.54 Å
(1) ESRF	BM	–	100	5.0	20.0	0.092	0.100	0.008	0.9	14	8×10^{12}	1×10^{13}
(2) ESRF	W	30	100	5.0	11.56	0.062	0.040	0.016	0.5	24	2.4×10^{14}	3×10^{14}
(3) ADONE (Frascati)	BM	–	100	1.5	5.0	0.8	0.4	0.04	8.0	1.5	2.4×10^{12}	5×10^{10}
(4) ADONE (Frascati)	W	6	100	1.5	2.6	1.4	0.24	0.08	4.3	3	1.4×10^{13}	3.4×10^{12}
(5) SRS (Daresbury)	BM	–	300	2.0	5.56	2.7	0.23	0.05	4.0	3	1×10^{13}	3×10^{12}
(6) SRS (Daresbury)	W	1	300	2.0	1.33	5.3	0.17	0.05	0.9	13	1×10^{13}	1.2×10^{13}
(7) DCI (Orsay)	BM	–	250	1.8	3.82	2.72	1.06	0.06	3.6	3.4	7×10^{12}	2.4×10^{12}
(8) DORIS (Hamburg)	BM	–	100	3.7	12.22	1.0	0.3	0.05	1.3	9.2	6×10^{12}	6.4×10^{12}
(9) DORIS (Hamburg)	BM	–	40	5.0	12.22	1.3	0.65	0.065	0.55	23	3×10^{12}	4.4×10^{13}
(10) DORIS (Hamburg)	W	32	100	3.7	20.57	1.5	0.4	0.033	2.3	5.5	1.9×10^{14}	1.3×10^{14}
(11) CESR (Cornell)	BM	–	40	5.5	32.0	1.44	1.0	0.065	1.0	11.5	3.5×10^{12}	4×10^{12}
(12) CESR (Cornell)	W	6	40	5.5	13.2	1.9	1.2	0.05	0.4	28	2×10^{13}	3×10^{13}
(13) NSLS X-ray (Brookhaven)	BM	–	300	2.5	6.83	0.25	0.1	0.01	2.4	5	1×10^{13}	8×10^{12}
(14) SPEAR	BM	–	100	3.0	12.7	2.0	0.28	0.05	2.7	5	5×10^{12}	3×10^{12}
(15) SPEAR	W	8	100	3.0	5.57	3.2	0.15	0.03	1.0	10	3.8×10^{13}	4.5×10^{13}
(16) SPEAR	W	54	100	3.0	8.36	3.2	0.15	0.03	1.7	7	2.6×10^{14}	2.4×10^{14}
(17) Photon Factory (Tsukuba)	BM	–	150	2.5	8.66	2.2	0.6	0.14	3.0	4	6×10^{12}	3×10^{12}
(18) Photon Factory (Tsukuba)	W	3	150	2.5	1.85	1.9	0.7	0.18	0.7	19	1.8×10^{13}	2.5×10^{13}
(19) VEPP-3	BM	–	100	2.2	6.15	6.15	0.08	0.02	3.0	4	3.5×10^{12}	1.5×10^{12}

* One standard deviation of Gaussian distribution.

with a frequency conversion system that shifts the peak power of the laser light from the infrared (1.054 μm) to the ultraviolet (0.351 μm) (Seka, Soures, Lund & Craxton, 1981). This led to a more efficient X-ray production, which permitted a more than twofold increase in X-ray flux, even though the maximum pulse energies had to be reduced to ~ 50 J to prevent damage to the optical components (Yaakobi, Boehli, Bourke, Conturie, Craxton, Delettrez, Forsyth, Frankel, Goldman, McCrory, Richardson, Seka, Shvarts & Soures, 1981). Forsyth & Frankel (1984) used the plasma X-ray source for diffraction studies with 4.45 Å X-rays with a focusing collimation system that delivered up to 10^{10} photons pulse^{-1} to the specimen over an area approximately 150 μm in diameter. More recently, by special target design (Forsyth, 1986, unpublished), fluxes have been increased by factors of 2 to 3 without altering the laser output. Other plasma sources have been described by Collins, Davanloo & Bowen (1986) and by Rudakov, Baigarin, Kalimin, Korolev & Kumachov (1991).

The cost of plasma sources is about an order of magnitude greater than that of rotating-anode generators (Nagel, 1980). Their use is at present confined to flash-diffraction experiments, since the duty cycle is a maximum of one flash every 30 min. Attempts are being made to increase the laser repetition rate; a substantial improvement could lead to a source that would rival storage-ring sources.

4.2.1.7. *Other sources of X-rays*

Parametric X-ray generation can be described as the diffraction of virtual photons associated with the field of a relativistic charged particle passing through a crystal. These diffracted photons appear as real photons with an energy that satisfies Bragg's law for the reflecting crystal planes, so that the energy can be tuned between 5 and 45 keV by rotating the mosaic graphite crystal. Linear accelerators with an energy between 100 and 500 MeV produce the incident relativistic electron beam (Maruyama, Di Nova, Snyder, Piestrup, Li, Fiorito & Rule, 1993; Fiorito, Rule, Piestrup, Li, Ho & Maruyama, 1993).

Transition-radiation X-rays with peak energies between 10 and 30 keV are produced when electrons from 100 to 400 MeV strike a stack of thin foils (Piestrup, Moran, Boyers, Pincus, Kephart, Gearhart & Maruyama, 1991). Quasi-monochromatic X-rays result from a selection of target foils with appropriate *K*-, *L*- or *M*-edge frequencies (Piestrup, Boyers, Pincus, Harris, Maruyama, Bergstrom, Caplan, Silzer & Skopic, 1991).

Table 4.2.1.7. *Intensity gain with storage rings over conventional sources; from Farge & Duke (1979), courtesy of ESF*

	GX6 rotating-anode tube 2.4 kW (Cu $K\alpha$ emission)	DCI 1.72 GeV and 240 mA	ESRF 5 GeV and 565 mA
Brightness impact ▲	Small-angle scattering with a double monochromator	×500 to 1000	×15000 to 3000
	Protein crystallography with a single-focus monochromator 1 mm^3 samples Small samples	 ×50 to 160 ×30 to 60	 ×900 to 1800 ×650 to 1300
	Diffuse scattering (wide angles, low resolution and large samples) with a curved graphite monochromator	×20 to 40	×160 to 320
Non characteristic wavelength (continuous background) EXAFS experimental set-up with a 100 kW rotating anode		×10^4	×10^5

Channelling radiation, resulting from the incidence of electrons with an energy of only about 5 MeV on appropriately aligned diamond or silicon crystals hold out the hope of producing a bright tunable X-ray source.

One or more of these methods may, in the future, be developed as X-ray sources that can compete with synchrotron-radiation sources.

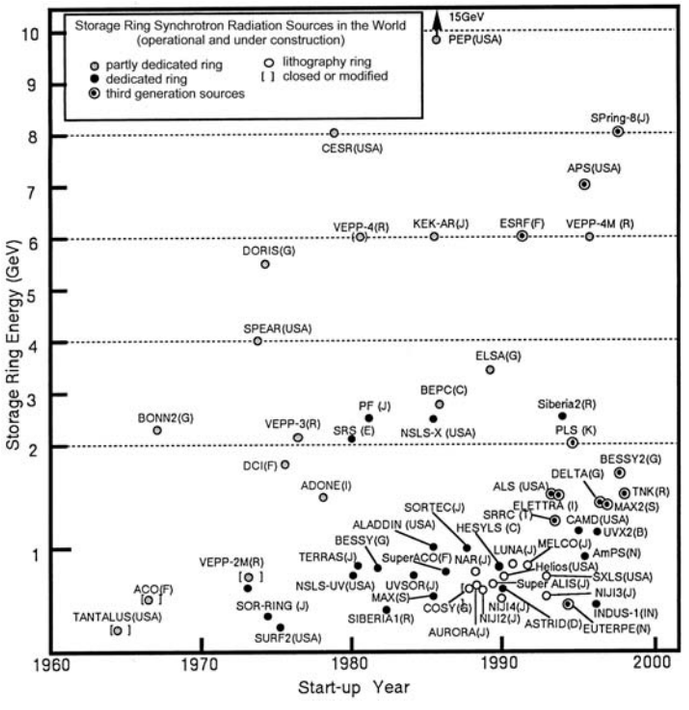

Fig. 4.2.1.11. The evolution of storage-ring synchrotron-radiation sources over the decades, as illustrated by their increasing number and range of machine energies (based on Suller, 1992).

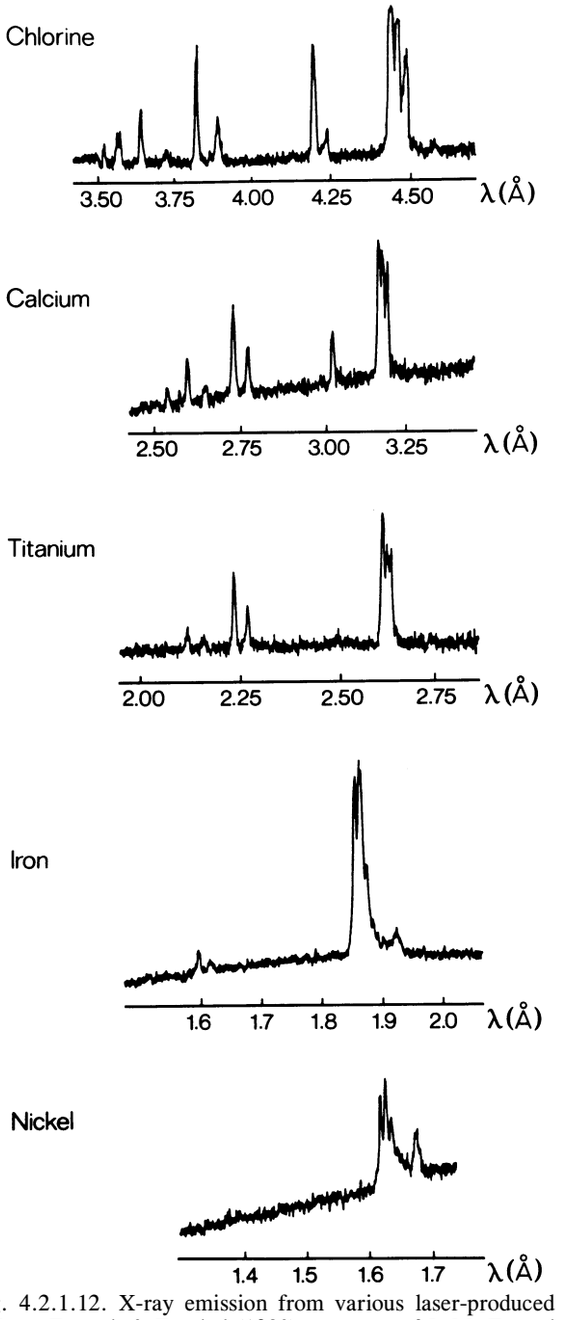

Fig. 4.2.1.12. X-ray emission from various laser-produced plasmas. From Forsyth & Frankel (1980); courtesy of J. M. Forsyth.

4.2.2. X-ray wavelengths (By R. D. Deslattes, E. G. Kessler Jr, P. Indelicato, and E. Lindroth)

4.2.2.1. *Historical introduction*

Wavelength tables in previous editions of this volume (Rieck, 1962; Arndt, 1992) were mainly obtained from the compilations prepared in Paris under the general direction of Professor Y. Cauchois (Cauchois & Hulubei, 1947; Cauchois & Senemaud, 1978). A separate effort by the late Professor J. A. Bearden and his collaborators (Bearden, 1967) has been widely used in other aggregations of tabular data and was made available for some time through the Standard Reference Data Program at the National Institute of Standards and Technology (NIST). For simplicity in the following discussion, we use the Bearden database as a frame of reference with respect to which our